

Article

SPH-Based Numerical Study on the Influence of Baffle Height and Inclination on the Interaction between Granular Flows and Baffles

Hualin Cheng¹, Bei Zhang¹ and Yu Huang^{1,2,*} 

¹ Department of Geotechnical Engineering, College of Civil Engineering, Tongji University, Shanghai 200092, China

² Key Laboratory of Geotechnical and Underground Engineering of the Ministry of Education, Tongji University, Shanghai 200092, China

* Correspondence: yhuang@tongji.edu.cn; Tel.: +86-21-6598-2384

Abstract: Arrays of baffles are widely used to prevent and mitigate granular flows (e.g., debris flows and landslides) in mountainous areas. A thorough understanding of the decelerating effect and the impact force of the baffle arrays is essential for engineering design and hazard mitigation. However, the interaction mechanism of granular flows and baffles is still not fully understood. In this work, numerical simulations based on the smoothed particle hydrodynamics (SPH) method are performed to investigate the influence of baffle height and inclination on the interaction between granular flows and baffles. It is found that the SPH model can well capture the flow kinematics of granular materials through the baffles and can obtain the impact force acting on the baffle structures. The results indicate that the performance of baffles is affected by the overflow of granular flows and increasing baffle height can effectively improve the deceleration effect on granular flows. However, the impact force analysis shows that the strength of higher baffle structures also needs to be increased in engineering design. In addition, the peak impact force is found to be closely related to the Froude number F_r .

Keywords: baffle arrays; granular flow; impact force; flow–structure interaction; smoothed particle hydrodynamics



Citation: Cheng, H.; Zhang, B.; Huang, Y. SPH-Based Numerical Study on the Influence of Baffle Height and Inclination on the Interaction between Granular Flows and Baffles. *Water* **2022**, *14*, 3063. <https://doi.org/10.3390/w14193063>

Academic Editors: Xingwei Ren, Zili Dai and Fangzhou Liu

Received: 6 September 2022

Accepted: 23 September 2022

Published: 29 September 2022

Publisher's Note: MDPI stays neutral with regard to jurisdictional claims in published maps and institutional affiliations.



Copyright: © 2022 by the authors. Licensee MDPI, Basel, Switzerland. This article is an open access article distributed under the terms and conditions of the Creative Commons Attribution (CC BY) license (<https://creativecommons.org/licenses/by/4.0/>).

1. Introduction

Granular flows such as debris flows and landslides occur frequently in mountainous areas [1]. It is well known that debris flows and landslides are always characterized by a large scale and high mobility. Therefore, such granular flows are among the most hazardous geological phenomena occurring in mountainous areas, causing heavy casualties and enormous economic losses [2,3]. To protect the downstream environment, ecology, and society (i.e., lives, property, infrastructure), engineering structures such as check dams, slit dams, and flexible barriers are often installed along the predicted flow path to impede granular flows [4–9]. Recently, an open barrier, the baffle arrays are of high interest to researchers or engineers. The baffle structure comprises rows of staggered baffles, strategically installed along the flow path of granular flows to reduce the damage. The shape of baffles can be rectangular and cylindrical. The primary function of baffles is to disrupt the flow pattern of the flow materials. When passing through the staggered baffles, the flow materials are impeded by the baffle structure. Furthermore, the mutual interference between the flow materials can also reduce their velocity. The kinetic energy of granular flows is greatly dissipated by the baffles. In addition, due to the obstruction of the baffle structures, part of the flow material is prevented from moving further downstream. Therefore, baffle arrays are viewed as an effective countermeasure in reducing the volume and the mobility of granular flows. The staggered arrays of baffles can be combined with check dams to reduce the impact force acting on the check dams [10,11]. In addition, baffles

can also be individually installed along the flow path to control the flow discharge and to decrease the final runout [12]. The baffle structures have been widely applied in the susceptible areas of debris flows [13–15] and snow avalanches [16,17]. In addition, the baffle structures are even used in hydraulic engineering [18].

An appropriate baffle design can effectively improve its performance compared with current empirical or normative methods. Therefore, it is essential to have a thorough understanding of the interaction mechanism between granular flows and baffles. The interaction mechanism between granular flows and baffles mainly involves the deceleration effect of baffles on granular flows and the impact of the granular flows acting on the baffles. This is also the basis for baffle design. Many flume model tests have been performed to investigate the interaction of particle flow with baffles [10–12,19–23]. For instance, Ng et al., [19] focused on the deceleration effect of baffles on granular flows and carried out a series of flume model tests to observe the influence of the layout of baffles. The results showed that the three baffle arrays reduced the runout distance and the frontal velocity by 65% and 57%, respectively. Choi et al., [20,21] and Law et al., [12] further investigated the interaction between granular flows and baffles under various baffle height, baffle space, and array space and finally gave the optimization recommendations. In addition, Wang et al., [22] performed a series of flume model tests with different baffle shapes (i.e., arc-shaped, cylinder-shaped, and cuboid-shaped) and found out that the arc-shaped baffles are more effective and economical than the other two. Based on small-scale model tests, Zhang et al., [23] demonstrated that the increase in the number of baffle arrays significantly reduced the flow mobility of granular material after passing the baffles. The results of the scaled physical experiments can help researchers and engineers better understand the interaction mechanisms and can provide the basis for the baffle design.

However, the physical experiment usually includes certain limitations for the analysis of the interaction between granular flows and baffles, such as the scale effect and the high cost. Moreover, numerical methods can obtain more detailed information about flow kinematics and interaction processes than scaling physical experiments. Recently, discrete element modeling (DEM) has been widely introduced to investigate the interaction between granular flow and baffles [11,20,23–26]. For instance, Bi et al., [24] used DEM to calculate the impact force acting on baffles under different baffle configurations and further analyzed the effect of the number and spacing of baffle columns and rows on the impact force. Zhou et al., [25] introduced DEM to investigate the run-up mechanism of granular flow after impacting on the baffles. Moreover, Zhang et al., [23] investigated the arch structure between the baffles at grain scale and further analyzed the effect of the Froude number on the flow–baffle interaction. In addition, the lattice Boltzmann method (LBM) [27] and the material point method (MPM) [28] have also been adopted for the numerical analysis of the deceleration effect of baffles on granular flows and the impact of the granular flows acting on the baffles. Different to the above discontinuum method or the particle-based continuum method, the smoothed particle hydrodynamics (SPH) method is a pure mesh-free Lagrangian method [29]. It is suitable for modeling the problem with a large deformation and a free surface. In addition, SPH is a continuum method and can efficiently calculate the large volume of granular flows. Accordingly, the SPH method has been widely used to model the dynamic behavior of granular flow (e.g., debris flow and landslide) along irregular terrain and to compute the impact force on the barrier structures [10,30–40]. Han et al., [30,31], Huang et al., [32], Tayyebi et al., [33], and Zhang and Xiao [34] used the SPH method to simulate the propagation and entrainment of large-scale debris flows. The promising results not only contribute to further understanding the flow mobility, but also provide a scientific basis for hazard assessments. Moreover, Dai et al., [35], Moriguchi et al., [36], Yang et al., [37], and Li et al., [10] successfully applied the SPH method to numerically study the fluid-like behavior of granular flows and the impact acting on the barrier structures. Considering the advantage in the numerical modeling of large-volume granular flow, this work used the SPH method combined with the Bingham model to investigate the interaction between granular flows and baffles. First, the SPH model is

adopted to model the dynamic behavior of granular flows with and without baffles. Then, the SPH model is further used to analyze the flow kinematics of granular flow under different baffle heights. Finally, the SPH method is applied to compute the impact force on baffles and to further analyze the influence of baffle height and the Froude number F_r on the distribution of the impact force along the baffle height and the peak impact force. This study provides an effective numerical approach to investigate the flow–baffle interaction and the findings of this work can provide a reliable basis for the engineering design of baffle arrays.

2. Materials and Methods

2.1. Governing Equations and Constitutive Model

The governing equations for granular flows in the SPH method adopt the classical Navier–Stokes equations, which consist of mass and momentum conservation equations. The Lagrangian descriptions are expressed as:

$$\frac{d\rho}{dt} = -\rho \nabla \cdot v \tag{1}$$

$$\frac{dv}{dt} = \frac{1}{\rho} \nabla \cdot \sigma + F \tag{2}$$

in which $\frac{d(\cdot)}{dt}$ is the material time derivative of (\cdot) , ∇ represents the gradient operator, ρ is the material density, v is the flow velocity vector, σ is the Cauchy stress tensor, and F is the external force vector.

Due to the fluid-like behavior of a granular flow, it can be treated as a visco-plastic fluid in numerical modeling [41,42]. Therefore, the total stress tensor σ is given as:

$$\sigma = -PI + \tau \tag{3}$$

in which P is an isotropic pressure, I is the identity matrix, and τ is the viscous stress tensor.

In this study, the isotropic pressure of the incompressible visco-plastic fluid is determined by the initial pressure and the dynamic pressure. The dynamic pressure here is obtained by an equation of state:

$$P_d = P_0 \left(\left(\frac{\rho}{\rho_0} \right)^m - 1.0 \right) \tag{4}$$

in which P_0 is the initial pressure, ρ_0 is the reference density, m represents the compressibility of the fluid, and the value of 7.0 is proven to be fit for simulation of incompressibility [35].

An appropriate constitutive model can enhance the reliability of the numerical simulation. The non-Newtonian Bingham fluid model shows good applicability in simulating the fluid-like behavior of granular flows. Therefore, the Bingham fluid model is adopted in this work to calculate the viscous stress of the granular flow as follows:

$$\tau = \eta \dot{\gamma} + \tau_{min} \tag{5}$$

in which η is the original viscosity, $\dot{\gamma}$ is the shear strain rate, and τ_{min} is the yield strength. For viscous fluid, the yield stress can be directly obtained by laboratory tests. For granular materials, the yield strength is usually determined by the shear strength parameter. Therefore, the Mohr–Coulomb criterion of $\tau_{min} = P \tan \varphi + c$ is adopted to calculate the yielding shear stress and further incorporated into the Bingham fluid model to calculate the viscous stress [36]. The modified Bingham fluid model is written as:

$$\tau = \eta \dot{\gamma} + P \tan \varphi + c \tag{6}$$

in which the shear strength parameter φ and c are the frictional angle and cohesion, respectively.

To further introduce the Bingham fluid model into the governing equations (Navier–Stokes equations), an equivalent Newtonian viscosity is introduced in the Bingham fluid model [43] as follows.

$$\eta' = \eta + (P \tan \varphi + c) / \dot{\gamma} \quad (7)$$

2.2. SPH Implementation

The Lagrangian-based SPH method is well suited for solving Navier–Stokes equations. The mesh-free SPH treats the computational domain as a series of contactless particles [44]. The arbitrarily distributed particles represent real material elements and carry the field variables of density, velocity, stress, etc. Based on the kernel approximation and the particle approximation of the SPH method, the field variable $f(x)$ and its gradient $\nabla f(x)$ of each particle are approximately calculated through summing the physical quantities of the neighboring particles within the supporting domain as:

$$f(x_i) = \sum_{j=1}^N f(x_j) \frac{m_j}{\rho_i} W_{ij} \quad (8)$$

$$\nabla f(x_i) = \sum_{j=1}^N f(x_j) \frac{m_j}{\rho_i} \nabla W_{ij} \quad (9)$$

in which subscripts i and j represent the concern particle and the neighboring particles within the supporting domain, N is the total number of particles within the influence domain, and m_j and ρ_j are the mass and density of the neighboring particles. $W_{ij} = W(x_i - x_j, h)$ is the smoothing kernel function using the positions of particles i and j , and h is the smoothing length determining the size of the smoothing kernel function. In this study, the B-spline function is adopted as the smoothing kernel function [45].

By using the SPH kernel approximation and particle approximation, the governing equations for granular flows can be rewritten as:

$$\frac{d\rho_i}{dt} = \sum_{j=1}^N m_j (v_i^\beta - v_j^\beta) \frac{\partial W_{ij}}{\partial x_i^\beta} \quad (10)$$

$$\frac{dv_i^\alpha}{dt} = \sum_{j=1}^N m_j \left(\frac{\sigma_i^{\alpha\beta} + \sigma_j^{\alpha\beta}}{\rho_i \rho_j} - \delta \Pi_{ij} \right) \frac{\partial W_{ij}}{\partial x_i^\beta} + g_i^\alpha \quad (11)$$

in which superscripts α and β represent the coordinate directions. To avoid the stress oscillation, an artificial viscosity term Π_{ij} is incorporated into the pressure term of the momentum Equation (11) [46].

In the SPH method, the boundary treatment cannot be directly imposed on the particles along the boundary of the computational domain, because the particle deficiency outside of the boundary will truncate the kernel approximation near the boundary, which always leads to inaccurate SPH interpolation. Therefore, extra boundary particles are created to address this issue. The boundary particles are used not only to prevent the fluid material particles from penetrating, but also to correct the SPH approximation in the incomplete supporting domain. In this study, the solid boundary is treated by a high-performance free-slip boundary method proposed by Tran et al., [47]. In this method, the boundary of the computational domain is represented by multiple layers of virtual SPH particles. These virtual boundary particles carry all basic information, just like normal SPH particles. The difference is that the properties of the boundary particles are obtained by direct interpolation of the neighboring fluid material particles instead of the governing equations. Then, the boundary particles participate in the normal SPH approximation for the field variables of the fluid material particles.

In this study, the governing equations of the granular flows are solved by the second Runge–Kutta time integrator. Obviously, the small size of the SPH particles of the three-

dimensional model and the small time step in numerical integration greatly increase the computational cost. Thus, parallel computing of the SPH model is carried out by the open multiprocessing (OpenMP) [46,48]. OpenMP supports multi-threading computing with shared memory. The main thread forks a series of sub-threads to which tasks are assigned for the concurrent execution on different processors. In addition, to further reduce the computing time and to further improve the computing efficiency, the linked-cell method was also used as the Nearest Neighbor Particle Search method to search the neighbor particles. More details about the SPH algorithms can be found in Cheng et al., [49]. The goodness of the proposed SPH numerical model for modeling the mass flow movement and the impact on the structures was tested in our previous studies [32,35,49].

In this study, an idealized model of the experimental scale is used in the SPH simulation to model and analyze the propagation of the granular flows and the impact on the baffle structures. In the actual conditions, a typical debris flow usually consists of the source area, the transportation area, and the accumulation area. Field investigation shows that the average inclination of the transportation area usually ranges from 20° to 60° [50]. The accumulation area is relatively flat terrain. Therefore, the flume adopted in the numerical simulations to model consists of two parts, which respectively represent the transportation area and the accumulation area. The source area is located at the top of the first channel. The simulation schematic is shown in Figure 1. Based on the terrain features of the transportation areas and the accumulation area, the inclination of the first and the second channel is set to be 40° and 0°, respectively. In addition, the numerical simulations are carried out on an experimental scale. Therefore, the length of the first channel is set to be 2.5 m, such that the granular flows have sufficient space to accelerate downstream. When moving to the second channel, the granular flows begin to slow down and accumulate. Then, a 1.0-m-long flume is used to model the accumulation area. To model the channelized flows, the height and width of the rectangular flume model are 0.35 m and 0.3 m, respectively. The arrays of baffles are perpendicularly installed at the end of the first channel. Three staggered arrays of baffles are considered for simplicity. The baffle dimensions are 30 mm × 30 mm. The height of baffles is set to be 100 mm. To distinguish baffle structures from slit dams, the transverse blockage needs to be controlled within 40% [5]. The transverse blockage is defined as the ratio of the total width of each baffle along the transverse direction and the channel width [20]. Then, the slit spacing in each array is set to be 60 mm. Thus, the transverse blockages of the three baffle arrays are 40%, 30%, and 40%, respectively. In addition, the array spacing is set to 90 mm to make the baffles form a square array. In the source area, the granular materials are initially fixed in a rectangular granular assembly, with a three-dimensional size of 0.5 m × 0.3 m × 0.26 m.

In the SPH numerical simulations, the chute channel system and the granular materials are discretized into SPH particles with the initial particle spacing of $\Delta x = 6$ mm to ensure the calculation accuracy and efficiency. The numerical model is discretized with a total of 305,967 SPH particles, including 144,884 granular flow particles and 161,083 fixed boundary particles for tbs. The granular flows simulated in the SPH simulations are assumed to be dry granular flows. In previous experimental research on the granular flows, the bulk density of the materials is 1400 kg/m³–1680 kg/m³ [19,23,51], and this work takes a value of 1520 kg/m³. As mentioned in Section 2.1, the granular flow is treated as a visco-plastic fluid and the non-Newtonian Bingham fluid model is adopted to model the fluid-like behavior of the granular flow. In the Bingham fluid model (Equation (5)), three mechanical parameters (i.e., cohesion, internal friction angle, and viscosity coefficient) are necessary for the SPH numerical simulations. The cohesion of the cohesionless granular flow is set to be zero. However, the internal friction angle of the granular flows has a wide range. In this study, the value of the internal friction angle is obtained by the parametric study. The results show that the value 22° can well capture the flow behavior of the granular flows through the baffles. In addition, in the Bingham fluid model, the viscosity coefficient of the granular flows can be set around 1.0 Pa·s [36,52]. Therefore, the viscosity coefficient takes a value of 1.0 Pa·s.

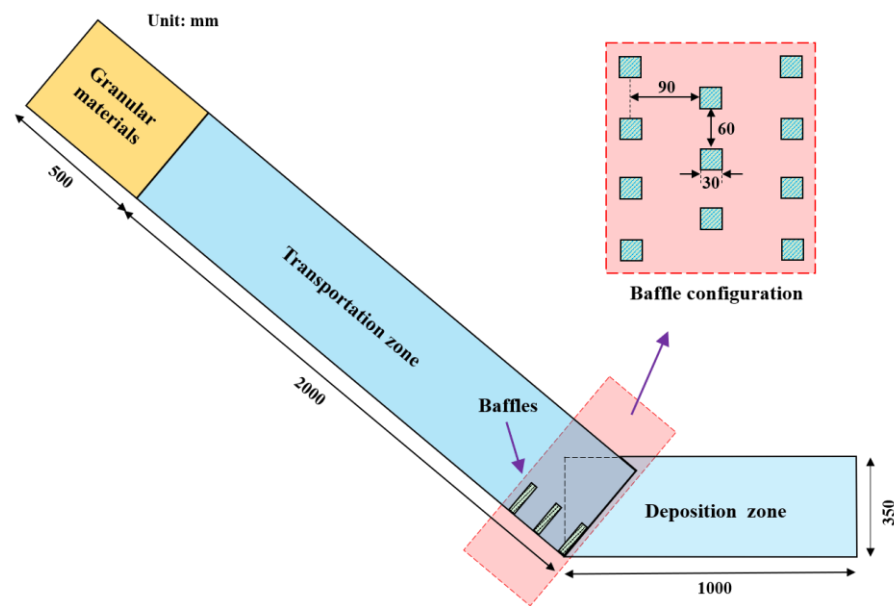


Figure 1. The simulation schematic of granular flow in a chute with baffles.

3. Results

3.1. Influence of Baffle on Flow Kinematics of Granular Flows

The dynamic behavior of a granular flow through the baffles is shown in Figure 2a–d. In addition, the granular flows in the flume without baffles are illustrated in Figure 2e–h. The initial time ($t = 0$ s) is also set as the moment when the flow front arrives at the section I–I'. At approximately 0.24 s, the flow front approaches the baffle at a high speed of 3.3 m/s. Then, the flow without baffles continues to accelerate towards the downstream until it reaches the accumulation zone and begins to slow down. However, when the flow impacts the first row of the baffles ($t = 0.4$ s), part of the flow passes through the baffle silts at a speed of less than 2.5 m/s and the rest of the flow is blocked by the baffles. In addition, the velocity of the flow front rapidly decreases after the flow passes between the second and the third arrays of the baffle. After $t = 2.1$ s, the granular flow has almost lost mobility, especially for the materials between and behind the baffles. The movement of the granular flows occurs mainly at the surface. Previous research on this flow behavior focused on the interaction between the particles of granular flows and reported that it is mainly controlled by the arch structure between the two adjacent columns of the baffles [23,53]. Nevertheless, the behavior of granular flows is described by the Bingham fluid model, so the effect of the arch structure is difficult to be accurately simulated here. The final runout distance of the two cases with and without baffles is 0.62 m and 0.75 m. The baffles effectively prevent the final runout of granular flows.

3.2. Influence of Baffle Height

The baffle height has been viewed as one of the major factors that influences the effectiveness of the baffles. Thus, another simulation of granular flow in a chute impeded by baffles with the same layout but different height of 0.20 m is carried out to analyze the effect of baffle height on the interaction between granular flow and baffles. First, Figure 3 provides particularly side and top-down views of the interaction between the granular flow and the baffles with a height of 0.1 m. Figure 3a shows that as the flow front impacts the first row of the baffles, the materials behind the baffles begin to run up along the baffles, and the materials flowing through the baffle silts immediately form a jet. Accordingly, as can be seen in the top-down view (Figure 3d), the three jets rush to the second row of the baffles. Soon after, the pile-up heights along the first and the second rows of the baffles continuously increase (Figure 3b); meanwhile, the three jets between the first and the second rows are further divided into four downstream jets moving to the last row of

the baffles (Figure 3e). Under the disturbance of the staggered baffles, the granular material flows out of the last row of the baffle at a speed of less than 1 m/s. As for the materials behind the baffles, part of the granular material continues to pile up along the baffles; the rest gradually forms the dead zone [54] at the base of the baffles. As the upstream granular material continues to move downward, the dead zone expands further upward. As a result, the subsequent flow runs up along the ramp of the dead zone and leads to overflow together with the previous pile-up material (Figure 3b,c). The overflow accelerates the flow front and has been viewed as one of the major factors influencing the effectiveness of baffles [5,11].

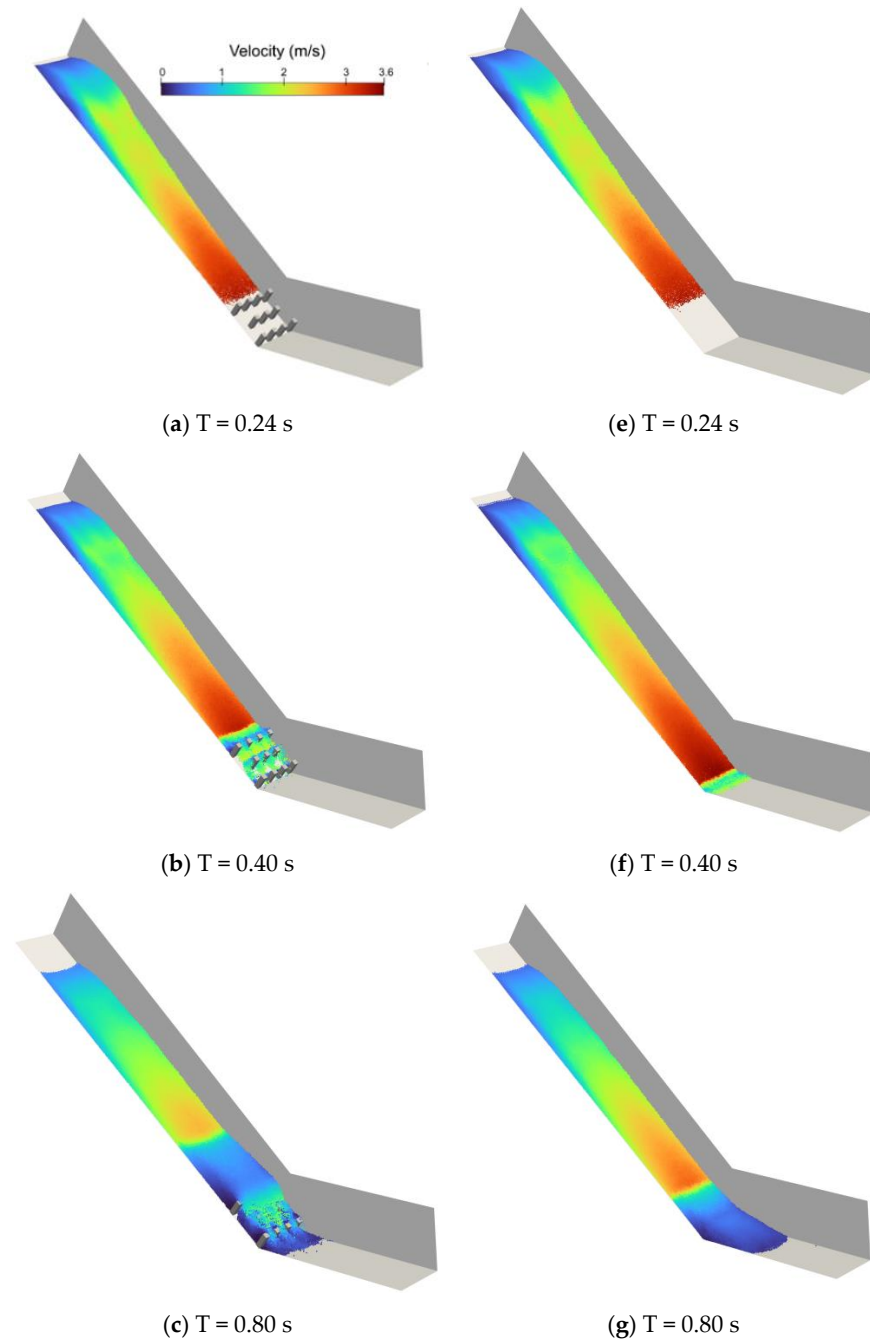


Figure 2. Cont.

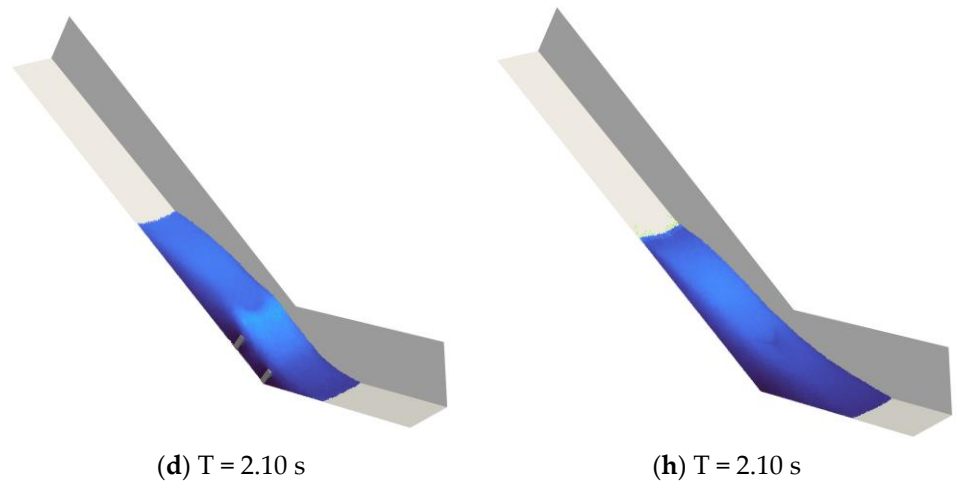


Figure 2. Simulated flow kinematics of granular flow with and without the obstruction of baffles: (a–d) with baffles and (e–h) without baffles.

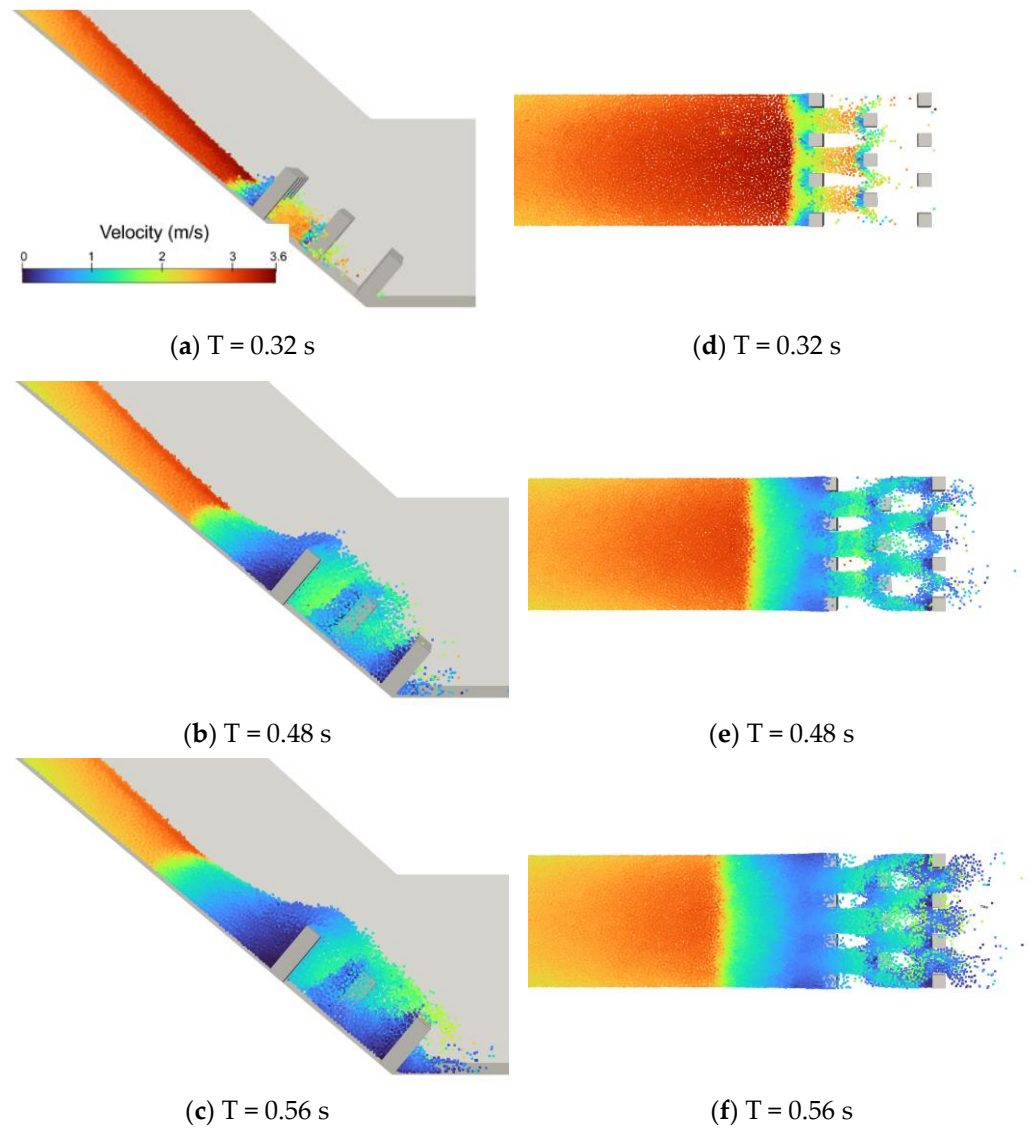


Figure 3. Flow kinematics of granular flow through the baffles: (a–c) side views and (d–f) top-down views.

Figure 4 shows the interaction process between the granular flow and the baffles with different heights. It is obvious that the overflow of the baffles with a height of 0.1 m occurs at approximately 0.4 s (Figure 4a). Before $t = 0.4$ s, the flow kinematics of the granular material are similar in the two cases of the baffles with heights of 0.1 m and 0.2 m. However, the flow kinematics become different when the granular material overflows the baffles with a height of 0.1 m. As can be seen in Figure 4b, the granular material overflowing the baffles is accelerated and moves to the deposition zone. However, the higher baffles effectively prevent the overflow and the granular material just downward flows between the slits (Figure 4d). In addition, the final runout distance is 0.62 m and 0.48 m in the two cases with 0.1 m and 0.2 m high baffles. The baffles with a height of 0.2 m can effectively prevent the overflow and further reduce the final runout.

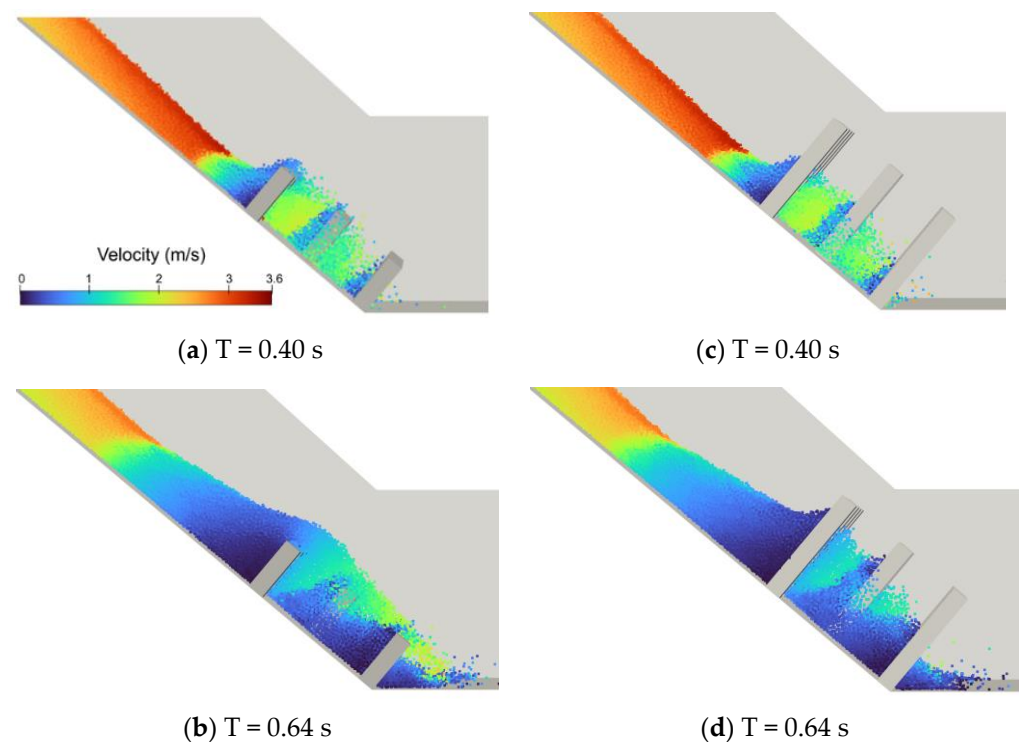


Figure 4. Comparison of the flow kinematics of the granular flow through 0.10 m and 0.20 m high baffles: (a,b) 0.1 m high baffles (c,d) 0.2 m high baffles.

3.3. Impact Force Analysis

The impact force of the flows on the baffles is the major factor that causes the failure of the baffles. In particular, the peak impact force on the baffles is an important basis for engineering design. Previous studies have shown that for the staggered baffles, the first row suffered greater impact force than the second and the third rows [11,23,24]. Therefore, this study focuses on the impact force on the surface of the first row of baffles. The impact force acting on the baffles is measured by the SPH approximation of the field variable of pressure. To get a full picture of the impact on baffles, impact forces (kPa) measured along the surface of 0.1 m and 0.2 m high baffles are illustrated in Figure 5. The positions of the measured point P1, P2, P3, and P4 are 12 mm, 36 mm, 60 mm, and 96 mm from the base of the 0.1 m and 0.2 m high baffles, respectively. Accordingly, the positions of the measured point P5, P6, and P7 are 144 mm, 168 mm, and 192 mm from the base of the 0.2 m high baffle, respectively. It is observed that the impact force on the bottom of the baffle is the largest. Furthermore, the peak impact force decreases along the height of the baffle and the corresponding arrival time increases. Particularly, when the granular flow climbs above 0.15 m of the baffles, the impact force acting on the baffles significantly reduces. It is worth noting that the impact force on the 0.1 m high baffles is slightly higher than that of the 0.2 m high baffles. In

addition, the total impact force (N) experienced by the first row of baffles with different heights is also calculated and illustrated in Figure 6. The peak value of the total impact force of the 0.1 m high and 0.2 m high baffles is approximately 30 N and 41 N, respectively, and the total impact force acting on the baffles is increased by approximately 37%. Therefore, although increasing the height of baffles can effectively improve the deceleration effect on the granular flow, the strength of the baffle structures also needs to be increased in the engineering design.

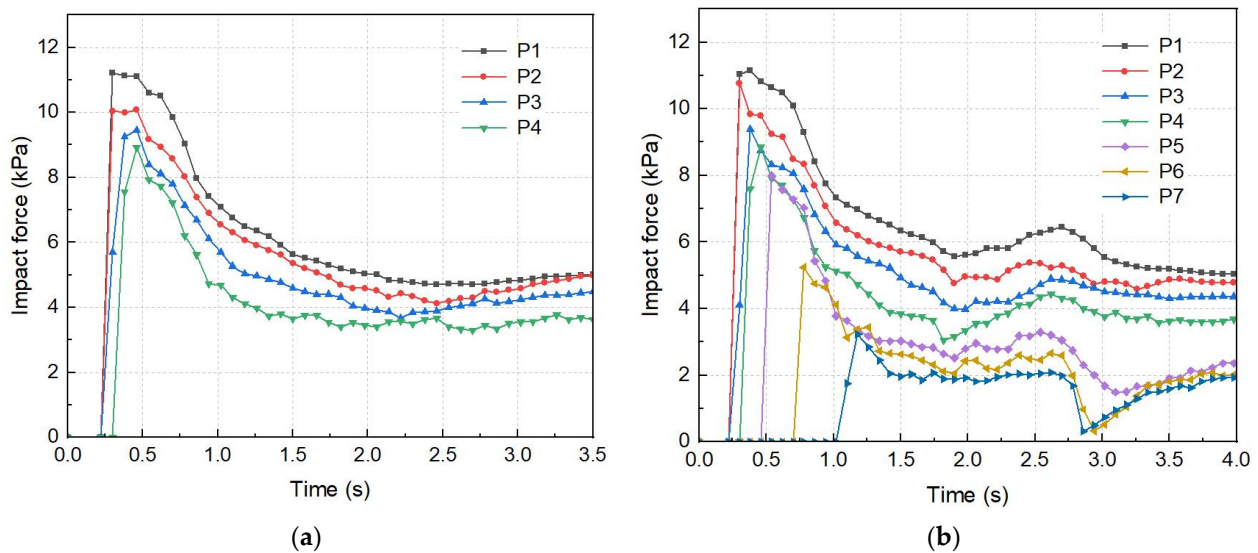


Figure 5. Impact forces along the surface of 0.1 m and 0.2 m high baffles: (a) 0.1 m high baffles and (b) 0.2 m high baffles.

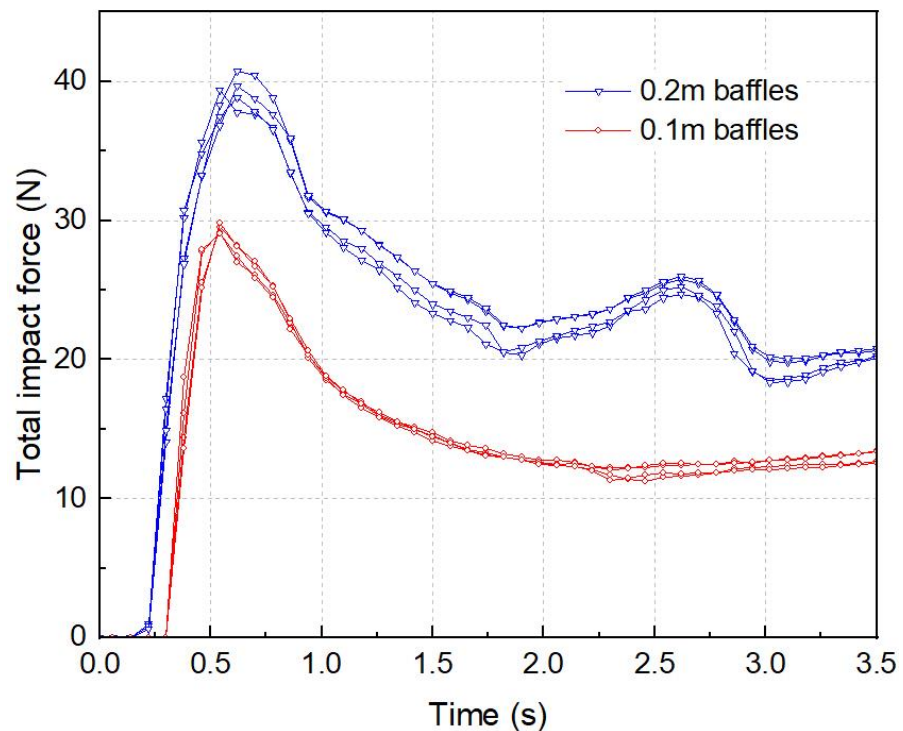


Figure 6. Total impact forces on the first row of the 0.1 m and 0.2 m high baffles.

In addition, the flume inclination is also an important factor affecting the impact force of the granular flow on the baffles. The effect of inclination on the impact effect is determined by the dimensionless Froude number F_r [23,55,56]. F_r indicates the ratio of inertial forces to gravitational forces and is determined by $F_r = v/\sqrt{gh\cos\theta}$, in which v is the velocity of the flow front, h is the flow depth, and θ is the flume inclination. In this study, SPH simulations are also performed for 30°, 35°, and 45° flume inclinations to observe the interaction between the granular flow and the baffles. First, the free flow without baffles under various inclinations is simulated to obtain the Froude number of the flow front before impacting the first row of baffles, which are 8.0, 11.0, and 15.8, respectively. In addition, the corresponding Froude number of the 40° flume inclination is 12.9. Obviously, F_r is proportional to the flume inclination. Furthermore, the simulation of granular flow impacting baffles under various inclinations is carried out to measure the impact force on the surface of the first row of baffles. The height of the baffles is 0.1 m. Figure 7 shows the impact force acting on 12 m from the base of the baffle. The peak impact force increases significantly with the increase in flume inclination. When the flume inclination increases to 45°, the peak impact force is almost three times that of the 30° flume inclination. In addition, the peak value of the total impact force and the impact force on the baffle of the first row under various inclinations is calculated and illustrated in Figure 8. It further indicates that the flume inclination has an obvious influence on the impact force acting on the baffles. As can be seen in Figure 8, the peak value of the impact force is proportional to the Froude number F_r .

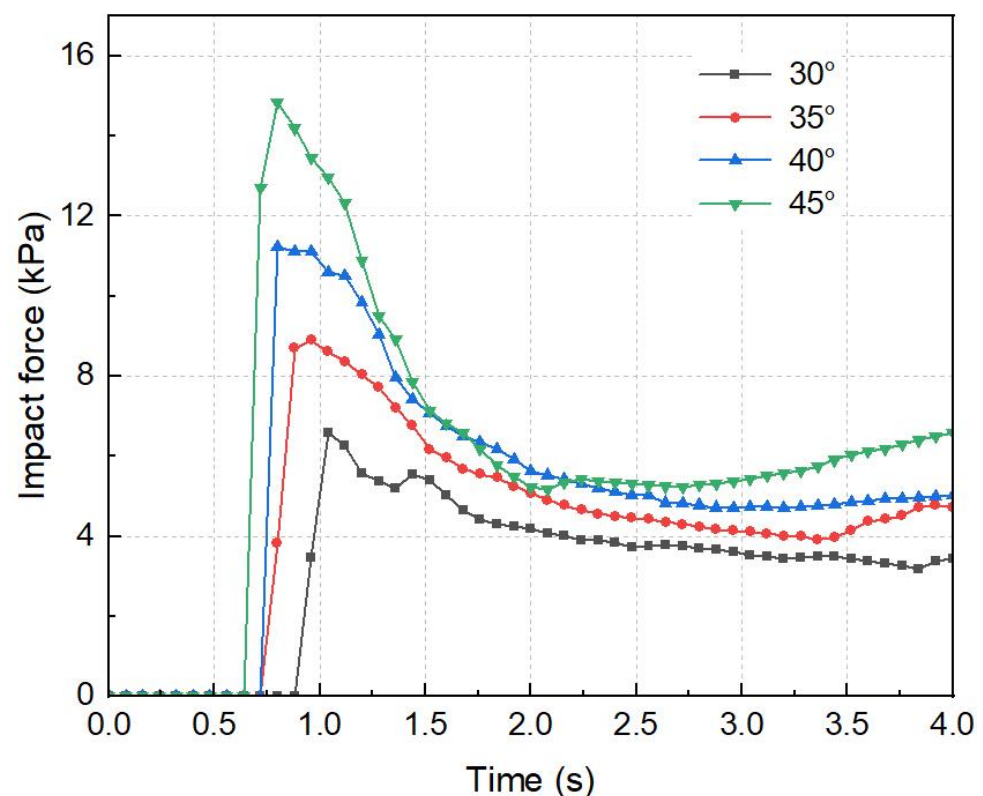


Figure 7. Comparison of the impact forces on the surface of 0.1 m high baffles on the various inclinations.

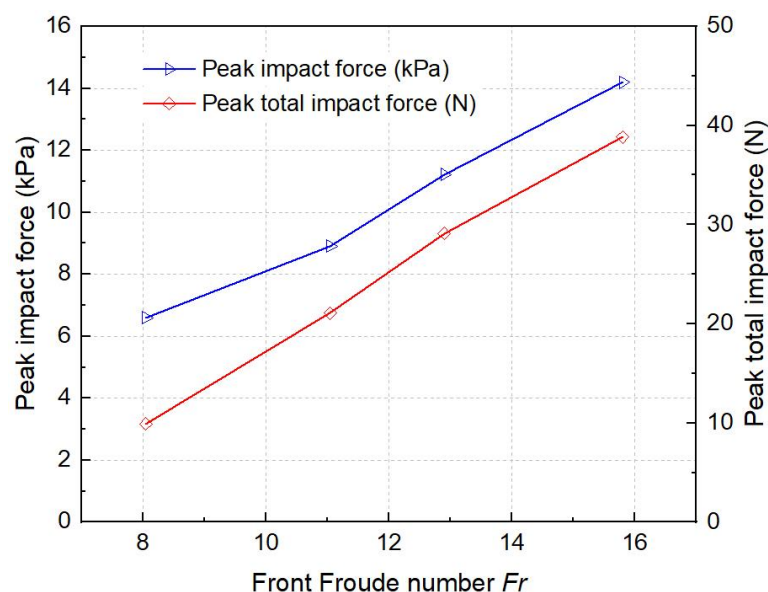


Figure 8. Peak total impact force and peak impact force on the baffle of the first row under various inclinations.

4. Discussion

Baffles have been viewed as an effective mitigation measure to reduce the destructivity of geohazards such as debris flows and landslides. In this paper, the SPH method combined with the Bingham fluid model is used to numerically study the interaction between granular flows and baffles on an experimental scale, trying to address the influence of the baffle height and the inclination on the flow–baffle interaction. The results (Figures 2 and 3) show that the SPH model can well capture the dynamic behavior of granular flows passing through the baffles that has been observed in the flume model tests conducted by Ng et al., [19] and Choi et al., [20] and in the numerical simulations conducted by Goodwin et al., [11] and Zhou et al., [25], including the jet flow between the baffle silts, the formation of a dead zone, the flows climbing along the baffles, and the overflow of granular materials. In addition, the results obtained by the SPH model clearly show that the change in flow patterns significantly decelerates the granular flows. However, the constitutive model adopted here cannot accurately simulate the effect of the soil arch structure between two baffles, which has been simulated in our previous DEM simulations [23] and is viewed as the major reason for the deceleration. In addition, the results obtained in this study verify that the height of baffles obviously affects the baffle performance [12,20,21]. Moreover, this study further indicates that the baffle performance can be effectively improved when the baffle height is raised to prevent the overflow. Both the results of the DEM simulations by Zhang and Huang [57] and the SPH simulations in this study show that the Froude characteristics against baffle arrays significantly affect the impact force on the baffles. In addition, the SPH method adopted in this study can further obtain the distributions of impact force along the baffles. The limitation of this paper is the lack of comparison with a physical chute experiment to further verify the parameters used in the SPH simulations. Hence, in future work, the efforts also need to be put into flume model tests to further improve the accuracy of the simulation results.

5. Conclusions

In this work, we have investigated the influence of baffle height and inclination on the interaction between granular flows and baffles using the SPH method. For this purpose, we have first investigated the interaction mechanism of granular flow and baffles by comparing the simulated results with and without baffles. The results reveal that the staggered baffle arrays significantly disrupt the flow front of the granular material and rapidly reduce

its velocity. Impeded by the baffles, the granular material behind the baffles forms the dead zone, and the subsequent flow runs up along the ramp of the dead zone and moves downward. We find that the overflow dominates the movement of the granular material in the final stage.

The influence of the baffle height has also been investigated by the SPH model. The results reveal that increasing the height of baffles can effectively prevent the overflow and decelerate the granular flows. With a baffle height of 0.2 m, the final runout distance of the granular flow is reduced by approximately 23% compared with the baffles with a height of 0.1 m.

The impact force on baffles is an important basis for engineering design. Here, we applied the SPH method to compute the impact force acting on baffles. The results reveal that, although increasing the height of baffles can effectively improve the deceleration effect on the granular flow, the strength of higher baffle structures also needs to be increased in engineering design. In addition, the influence of the flume inclination on the impact force has been investigated. As the flume inclination increases, the Froude number F_r of the flow front increases, which significantly increases the impact force on the baffles. Both the peak impact force (kPa) and the peak total impact force (N) are proportional to the Froude number F_r .

Author Contributions: Conceptualization, H.C., Y.H. and B.Z.; methodology, H.C. and Y.H.; data curation, H.C. and B.Z.; formal analysis, H.C.; writing—original draft preparation, H.C.; writing—review and editing, Y.H. and B.Z.; funding acquisition, H.C. and Y.H. All authors have read and agreed to the published version of the manuscript.

Funding: This work was supported by the National Natural Science Foundation of China (Grant Nos. 41807284 and 41831291).

Conflicts of Interest: The authors declare no conflict of interest.

References

- Hungr, O.; Leroueil, S.; Picarelli, L. The Varnes classification of landslide types, an update. *Landslides* **2013**, *11*, 167–194. [[CrossRef](#)]
- Zhu, C.; Huang, Y.; Sun, J. Solid-like and liquid-like granular flows on inclined surfaces under vibration—Implications for earthquake-induced landslides. *Comput. Geotech.* **2020**, *123*, 103598. [[CrossRef](#)]
- Ji, F.; Dai, Z.; Li, R. A multivariate statistical method for susceptibility analysis of debris flow in southwestern China. *Nat. Hazard Earth Sys.* **2020**, *20*, 1321–1334. [[CrossRef](#)]
- Mizuyama, T. Structural countermeasures for debris flow disasters. *Int. J. Erosion. Control. Eng.* **2008**, *1*, 38–43. [[CrossRef](#)]
- Ng, C.W.W.; Song, D.; Choi, C.E.; Liu, L.H.D.; Kwan, J.S.H.; Koo, R.C.H.; Pun, W.K. Impact mechanisms of granular and viscous flows on rigid and flexible barriers. *Can. Geotech. J.* **2017**, *54*, 188–206. [[CrossRef](#)]
- Li, X.; Zhao, J. A unified CFD-DEM approach for modeling of debris flow impacts on flexible barriers. *Int. J. Numer. Anal. Methods Geomech.* **2018**, *42*, 1643–1670.
- Zhou, G.G.D.; Hu, H.S.; Song, D.; Zhao, T.; Chen, X.Q. Experimental study on the regulation function of slit dam against debris flows. *Landslides* **2019**, *16*, 75–90. [[CrossRef](#)]
- Song, D.; Choi, C.E.; Ng, C.W.W.; Zhou, G.G.D. Geophysical flows impacting a flexible barrier: Effects of solid-fluid interaction. *Landslides* **2018**, *15*, 99–110. [[CrossRef](#)]
- Zhu, C.; Chen, Z.; Huang, Y. Coupled moving particle simulation–finite-element method analysis of fluid–structure interaction in geodisasters. *Int. J. Geomech.* **2021**, *21*, 04021081. [[CrossRef](#)]
- Li, S.; Peng, C.; Wu, W.; Wang, S.; Chen, X.; Chen, J.; Zhou, G.G.D.; Chitneedi, B.K. Role of baffle shape on debris flow impact in step-pool channel: An SPH study. *Landslides* **2020**, *17*, 2099–2111. [[CrossRef](#)]
- Goodwin, G.R.; Choi, C.E.; Yune, C.Y. Towards rational use of baffle arrays on sloped and horizontal terrain for filtering boulders. *Can. Geotech. J.* **2021**, *58*, 1571–1589. [[CrossRef](#)]
- Law, P.H. Computational Study of Granular Debris Flow Impact on Rigid Barriers and Baffles. Ph.D. Thesis, The Hong Kong University of Science and Technology Civil and Environmental Engineering, Hong Kong, 2015.
- Cosenza, E.; Cozzolino, L.; Pianese, D.; Fabbrocino, G.; Acanfora, M. Concrete structures for mitigation of debris-flow hazard in the Montoro Inferiore Area, Southern Italy. In *2nd International Congress*; International Federation for Structural Concrete: Naples, Italy, 2006; pp. 1–12.
- Hu, H.; Zhou, G.G.D.; Song, D.; Cui, K.F.E.; Huang, Y.; Choi, C.E.; Chen, H. Effect of slit size on the impact load against debris-flow mitigation dams. *Eng. Geol.* **2020**, *274*, 105764. [[CrossRef](#)]
- Choi, C.E.; Ng, C.W.W.; Law, P.H.; Song, D.; Kwan, J.H.S.; Ho, K.K.S. Computational investigation of baffle configuration on impedance of channelized debris flow. *Can. Geotech. J.* **2015**, *52*, 182–197. [[CrossRef](#)]

16. Hakonardottir, K.M. The Interaction between Snow Avalanches and Dams. Ph.D. Thesis, University of Bristol, School of Mathematics, Bristol, UK, 2004.
17. Mast, C.M.; Arduino, P.; Miller, G.R.; Mackenzie-Helnwein, P. Avalanche and landslide simulation using the material point method: Flow dynamics and force interaction with structures. *Computat. Geosci.* **2014**, *18*, 817–830. [[CrossRef](#)]
18. Thompson, P.L.; Kilgore, R.T. *Hydraulic Design of Energy Dissipators for Culverts and Channels: Hydraulic Engineering Circular Number 14 (No. FHWA-NHI-06-086)*; National Highway Institute (US): San Diego, CA, USA, 2006.
19. Ng, C.W.W.; Choi, C.E.; Song, D.; Kwan, J.H.S.; Koo, R.C.H.; Shiu, H.Y.K.; Ho, K.K.S. Physical modeling of baffles influence on landslide debris mobility. *Landslides* **2015**, *12*, 1–18. [[CrossRef](#)]
20. Choi, C.E. Flume and Discrete Element Investigation of Granular Flow Mechanisms and Interaction with Baffles. Ph.D. Thesis, The Hong Kong University of Science and Technology Civil and Environmental Engineering, Hong Kong, 2013.
21. Choi, C.E.; Ng, C.W.W.; Song, D.; Kwan, J.H.S.; Shiu, H.Y.K.; Ho, K.K.S.; Koo, R.C.H. Flume investigation of landslide debris-resisting baffles. *Can. Geotech. J.* **2014**, *51*, 540–553. [[CrossRef](#)]
22. Wang, D.; Li, Q.; Bi, Y.; He, S. Effects of new baffles system under the impact of rock avalanches. *Eng. Geol.* **2020**, *264*, 105261. [[CrossRef](#)]
23. Zhang, B.; Huang, Y.; Liu, J. Micro-mechanism and efficiency of baffle structure in deceleration of granular flows. *Acta Geotech.* **2021**, *16*, 3667–3688. [[CrossRef](#)]
24. Bi, Y.; Du, Y.; He, S.; Sun, X.; Wang, D.; Li, X.; Liang, H.; Wu, Y. Numerical analysis of effect of baffle configuration on impact force exerted from rock avalanches. *Landslides* **2018**, *15*, 1029–1043. [[CrossRef](#)]
25. Zhou, G.G.D.; Du, J.; Song, D.; Choi, C.E.; Hu, H.; Jiang, C. Numerical study of granular debris flow run-up against slit dams by discrete element method. *Landslides* **2020**, *17*, 585–595. [[CrossRef](#)]
26. Law, P.H.; Choi, C.E.; Ng, C.W.W. Discrete-element investigation of influence of granular debris flow baffles on rigid barrier impact. *Can. Geotech. J.* **2016**, *53*, 179–185. [[CrossRef](#)]
27. Bi, Y.; Wang, D.; Fu, X.; Lin, Y.; Sun, X.; Jiang, Z. Optimal array layout of cylindrical baffles to reduce energy of rock avalanche. *J. Mt. Sci.* **2022**, *19*, 493–512. [[CrossRef](#)]
28. Li, X.; Yan, Q.; Zhao, S.; Luo, Y.; Wu, Y.; Wang, D. Investigation of influence of baffles on landslide debris mobility by 3D material point method. *Landslides* **2020**, *17*, 1129–1143. [[CrossRef](#)]
29. Lucy, L.B. A numerical approach to the testing of the fission hypothesis. *Astron. J.* **1977**, *82*, 1013–1024. [[CrossRef](#)]
30. Han, Z.; Su, B.; Li, Y.; Dou, J.; Wang, W.; Zhao, L. Modeling the progressive entrainment of bed sediment by viscous debris flows using the three-dimensional SC-HBP-SPH method. *Water Res.* **2020**, *182*, 116031. [[CrossRef](#)]
31. Han, Z.; Yang, F.; Li, Y.; Dou, J.; Chen, N.; Hu, G.; Chen, G.; Xu, L. GIS-based three-dimensional SPH simulation for the 11 april 2018 yabakei landslide at oita nakatsu, Japan. *Water* **2021**, *13*, 3012. [[CrossRef](#)]
32. Huang, Y.; Cheng, H.; Dai, Z.; Xu, Q.; Liu, F.; Sawada, K.; Moriguchi, S.; Yashima, A. SPH-based numerical simulation of catastrophic debris flows after the 2008 Wenchuan earthquake. *B Eng. Geol. Environ.* **2015**, *74*, 1137–1151. [[CrossRef](#)]
33. Tayyebi, S.M.; Pastor, M.; Stickle, M.M. Two-phase SPH numerical study of pore-water pressure effect on debris flows mobility: Yu Tung debris flow. *Comput. Geotech.* **2021**, *132*, 103973. [[CrossRef](#)]
34. Zhang, W.; Xiao, D. Numerical analysis of the effect of strength parameters on the large-deformation flow process of earthquake-induced landslides. *Eng. Geol.* **2019**, *260*, 105239. [[CrossRef](#)]
35. Dai, Z.; Huang, Y.; Cheng, H.; Xu, Q. SPH model for fluid–structure interaction and its application to debris flow impact estimation. *Landslides* **2017**, *14*, 917–928. [[CrossRef](#)]
36. Moriguchi, S.; Borja, R.I.; Yashima, A.; Sawada, K. Estimating the impact force generated by granular flow on a rigid obstruction. *Acta Geotech.* **2009**, *4*, 57–71. [[CrossRef](#)]
37. Yang, E.; Bui, H.H.; Nguyen, G.D.; Choi, C.E.; Ng, C.W.W.; De Sterck, H.; Bouazza, A. Numerical investigation of the mechanism of granular flow impact on rigid control structures. *Acta Geotech.* **2021**, *16*, 2505–2527. [[CrossRef](#)]
38. Bui, H.H.; Kodikara, J.K.; Bouazza, A.; Haque, A.; Ranjith, P.G. A novel computational approach for large deformation and post-failure analyses of segmental retaining wall systems. *Int. J. Numer. Anal. Methods Géoméch.* **2014**, *38*, 1321–1340. [[CrossRef](#)]
39. Huang, Y.; Jin, X.; Ji, J. Effects of barrier stiffness on debris flow dynamic Impact—II: Numerical simulation. *Water* **2022**, *14*, 182. [[CrossRef](#)]
40. Sheikh, B.; Qiu, T.; Ahmadipur, A. Comparison of SPH boundary approaches in simulating frictional soil–structure interaction. *Acta Geotech.* **2021**, *16*, 2389–2408. [[CrossRef](#)]
41. Hosseini, K.; Omidvar, P.; Kheirkhahan, M.; Farzin, S. Smoothed particle hydrodynamics for the interaction of Newtonian and non-Newtonian fluids using the μ (I) model. *Powder Technol.* **2019**, *351*, 325–337. [[CrossRef](#)]
42. Massoudi, M.; Phuoc, T.X. Conduction and dissipation in the shearing flow of granular materials modeled as non-Newtonian fluids. *Powder Technol.* **2007**, *175*, 146–162. [[CrossRef](#)]
43. Uzuoka, R.; Yashima, A.; Kawakami, T.; Konrad, J.M. Fluid dynamics based prediction of liquefaction induced lateral spreading. *Comput. Geotech.* **1998**, *22*, 243–282. [[CrossRef](#)]
44. Liu, M.; Liu, G. Smoothed particle hydrodynamics (SPH): An overview and recent developments. *Arch. Comput. Method E* **2010**, *17*, 25–76. [[CrossRef](#)]
45. Monaghan, J.J.; Lattanzio, J.C. A refined particle method for astrophysical problems. *Astron. Astrophys.* **1985**, *149*, 135–143.

46. Zhang, W.; Maeda, K.; Saito, H.; Li, Z.; Huang, Y. Numerical analysis on seepage failures of dike due to water level-up and rainfall using a water–soil-coupled smoothed particle hydrodynamics model. *Acta Geotech.* **2016**, *11*, 1401–1418. [[CrossRef](#)]
47. Tran, H.T.; Wang, Y.; Nguyen, G.D.; Kodikara, J.; Sanchez, M.; Bui, H.H. Modelling 3D desiccation cracking in clayey soils using a size-dependent SPH computational approach. *Comput. Geotech.* **2019**, *116*, 103209. [[CrossRef](#)]
48. Zhang, W.; Ji, J.; Gao, Y. SPH-based analysis of the post-failure flow behavior for soft and hard interbedded earth slope. *Eng. Geol.* **2020**, *267*, 105446. [[CrossRef](#)]
49. Cheng, H.; Huang, Y.; Zhang, W.; Xu, Q. Physical process-based runout modeling and hazard assessment of catastrophic debris flow using SPH incorporated with ArcGIS: A case study of the Hongchun gully. *Catena* **2022**, *212*, 106052. [[CrossRef](#)]
50. Iverson, R.M.; Reid, M.E.; LaHusen, R.G. Debris-flow mobilization from landslides. *Annu. Rev. Earth Planet. Sci.* **1997**, *25*, 85–138. [[CrossRef](#)]
51. Huang, Y.; Jin, X.; Ji, J. Effects of barrier stiffness on debris flow dynamic impact—I: Laboratory flume test. *Water* **2022**, *14*, 177. [[CrossRef](#)]
52. Salehizadeh, A.M.; Shafiei, A.R. Modeling of granular column collapses with μ (I) rheology using smoothed particle hydrodynamic method. *Granul. Matter.* **2019**, *21*, 1–18. [[CrossRef](#)]
53. Azema, E.; Radjai, F. Force chains and contact network topology in sheared packings of elongated particles. *Phys. Rev. E* **2012**, *85*, 031303. [[CrossRef](#)] [[PubMed](#)]
54. Nguyen, N.H.; Bui, H.H.; Nguyen, G.D. Effects of material properties on the mobility of granular flow. *Granul. Matter.* **2020**, *22*, 1–17. [[CrossRef](#)]
55. Song, D.; Zhou, G.G.D.; Xu, M.; Choi, C.E.; Li, S.; Zheng, Y. Quantitative analysis of debris-flow flexible barrier capacity from momentum and energy perspectives. *Eng. Geol.* **2019**, *251*, 81–92. [[CrossRef](#)]
56. Jiang, Y.; Towhata, I. Experimental study of dry granular flow and impact behavior against a rigid retaining wall. *Rock Mech. Rock Eng.* **2013**, *46*, 713–729. [[CrossRef](#)]
57. Zhang, B.; Huang, Y. Numerical and analytical analyses of the impact of monodisperse and bidisperse granular flows on a baffle structure. *Landslides* **2022**. [[CrossRef](#)]